Enhancing the Sensitivity of Percolative Graphene Films for Flexible and Transparent Pressure Sensor Arrays

Zhuo Chen, Tian Ming, Mahomed Mehdi Goulamaly, Heming Yao, Daniel Nezich, Marek Hempel, Mario Hofmann, and Jing Kong**

Flexible and transparent pressure sensor arrays can find applications in many places such as touch panels, artificial skin, or human motion detection. However, conventional strain gauges are rigid and opaque and are not suitable for such applications. Graphene-based percolative strain gauges can overcome these challenges but currently are still in the infancy of their development. In this work, the performance of graphene-based percolative strain gauges is investigated and guidelines to improve the durability and sensitivity of graphene films as sensing elements are developed. It is found that the gauge factor depends on the initial resistance of the graphene film. For the same film resistance, it is found that graphene flake size and film morphology also play a role in determining the gauge factor. Increasing the flake–flake resistance through assembly of surfactant molecules between graphene flakes provides an additional route to enhance the gauge factor. Furthermore, encapsulating the percolative film in micrometer-thin Poly(methyl methacrylate) does not disrupt the sensing process but significantly improves the sensor's durability. Finally, thus enhanced graphene strain gauges are integrated into flexible and transparent pressure sensor arrays that exhibit high reproducibility and sensitivity.

1. Introduction

Pressure sensor arrays, which can sense pressure in a position-resolved manner, are essential to mimicking tactile perception, also called the sense of touch. Adding flexibility and transparency to pressure sensor arrays is a promising route for mobile electronics, wearable electronics, and implantable electronics,[1] with applications in flexible touch panel,[2–4] artificial skin,[5–12] and human motion detection.[13–17] Pressure sensors are in general based on pressure induced strain and the corresponding changes in electric resistance,[18] capacitance,[19] or potential.[20] They are usually rigid and bulky. Recently, significant progress has been reported in making smaller, more flexible, and more sensitive pressure sensor based on novel materials, including conductive polymers,[4,11] semiconducting nanowires,[21] metal nanowires,[17] carbon nanotubes,[10,15] graphene,[22,23] etc. Those materials enable unique properties like flexibility and transparency due to their small footprint, unique electrical properties, small optical cross section, and high aspect ratio.[1] A detailed summary of various strain gauges or pressure sensors based on different materials is presented in Table S1 (Supporting Information).

In 2012, we developed a novel class of strain gauges based on thin films of percolative networks of 2D materials.[24] The sensing mechanism is based on strain-dependent film morphology changes. We chose exfoliated graphene-flake thin films, because they can be produced from graphite at large scale and low cost.[25] Percolative networks of graphene can be obtained by the assembly of graphene flakes with high enough density so that overlap between neighboring flakes occurs. The percolative graphene film strain gauges are less than 100 nm thin, flexible, and semi-transparent. Different from traditional strain gauges, the device sensitivity as expressed by the gauge factor (GF) was found to scale with initial resistance following a power-law dependence, which enables a unique control over the sensor's performance. Despite the potential of this approach, practical applications remain elusive due to the limited understanding of the impact of processing conditions and material properties on scaling dependence.

Z. Chen, Dr. T. Ming, M. M. Goulamaly, Dr. J. Kong
Research Laboratory of Electronics
Massachusetts Institute of Technology
Cambridge, MA 02139, USA
E-mail: tming@mit.edu; jingkong@mit.edu
H. Yao
Sino-French Engineer School
Beihang University
Beijing, China
Dr. D. Nezich
Lincoln Laboratory
Massachusetts Institute of Technology
Lexington, MA 02421, USA
M. Hempel, Dr. J. Kong
Department of Electrical Engineering and Computer Science
Massachusetts Institute of Technology
Cambridge, MA 02139, USA
Dr. M. Hofmann
Department of Materials Science and Engineering
National Cheng Kung University
Tainan, Taiwan

DOI: 10.1002/adfm.201503674

In this work, the factors governing the scaling dependence and reliability of percolative graphene strain sensors are identified. Based on this understanding, highly reliable and sensitive pressure sensors are produced and applied in flexible and transparent pressure sensor arrays. This work improves the potential of percolative strain sensors to replace existing pressure sensors and enable novel application in sensor array technologies.

2. Results

2.1. The Effect of Graphene Flake Size

One major factor contributing to the conductivity of percolative films is the dimension of its constituents.[26,27] Atomic force microscopy (AFM) was employed to image individual graphene flakes deposited on SiO_2/Si wafer. Sizes and thicknesses of 100 graphene flakes for each solution were collected, and plotted into histograms (**Figure 1**a–d). The statistics show that electrochemical exfoliation (EE) graphene exhibits average flake size of 1.1 ± 0.4 µm (Figure 1a), and solvent exfoliation (SE) graphene has average size of 90 ± 26 nm (Figure 1c). To obtain graphene with flake size between 90 nm and 1.1 µm, we break down the EE graphene flakes into smaller pieces by sonication. 40 h sonication was performed and graphene with 170 ± 50 nm (Figure 1b) flake sizes were obtained. Subsequently, we denote the 1.1 µm and 170 nm EE graphene samples as EE and EE-small, respectively. Figure 1e shows the normalized Raman spectra of the three graphene samples. All the spectra exhibit a pronounced D peak and a distinguishable D′ peak, indicating the high density of defects generated during the exfoliation procedure.[28] The additional sonication, however, seems to not increase the defectiveness significantly as indicated by the similarity in the Raman spectra of the two EE samples. For each of the three samples, the amount of graphene sprayed was varied in order to obtain percolative films with different initial resistance ranging from 10^4 to 10^7 ohm. Films with larger resistance show higher transparency, which accords well with less material being sprayed and thus fewer conductive channels (Figure 1f).

The measured GFs for all different flake sizes are plotted as a function of initial resistance in Figure 1g. Films from all three groups of graphene samples exhibit increasing GF with decreasing graphene flake density and larger initial resistance, which is consistent with our previous work.[24] Furthermore, the observed slopes are similar irrespective of the flake dimension or production process. Conversely, the GF intercepts with y-axis for the three types of samples exhibit large differences. A clear trend between the average flake dimension and the intercept can be observed (Figure 1g).

This observation can be intuitively explained by a simplified conducting model of the percolative network. The total resistance of the network consists of the resistance within individual graphene flakes (in-plane resistance) and the resistance between two touching graphene flakes (out-of-plane resistance). According to our previous simulations,[24] the increase of

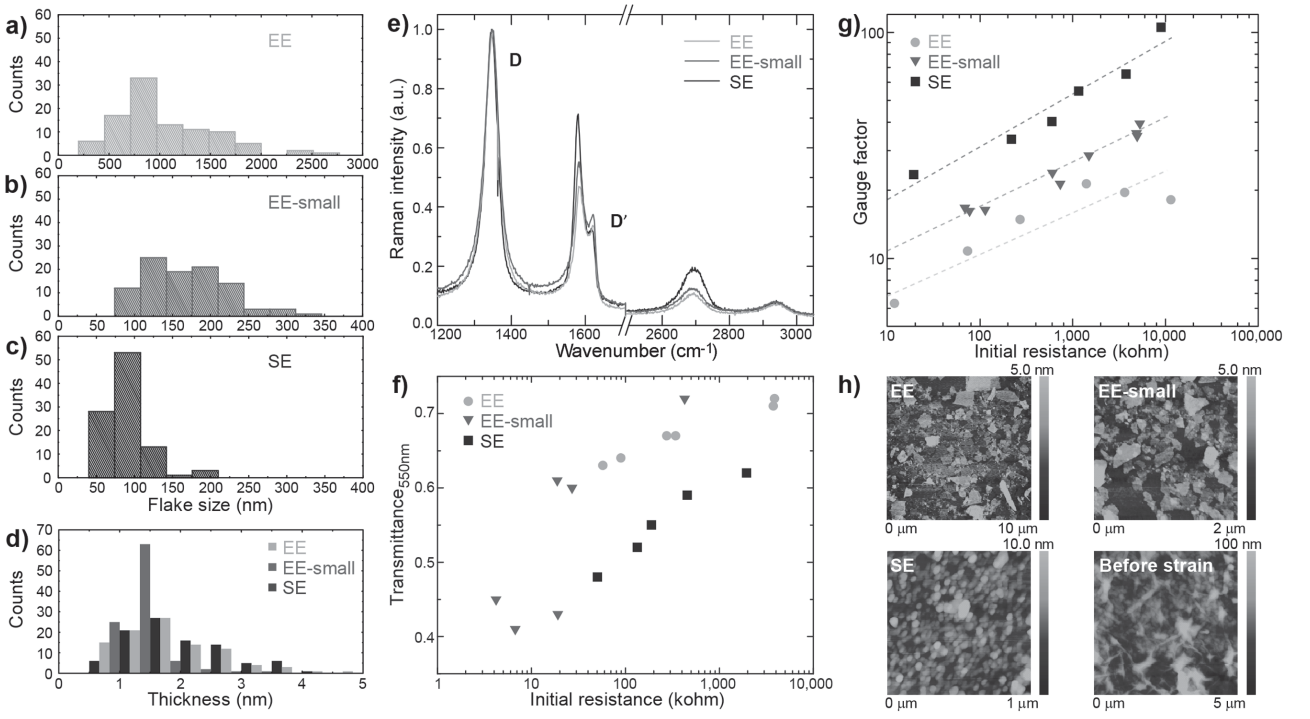

Figure 1. The effect of graphene flake size on GF. a–c) Flake size distributions of EE, EE-small, and SE graphene samples. d) The thicknesses of EE, EE-small, and SE graphene samples are 1.8 ± 0.8 nm, 1.2 ± 0.4 nm, and 2.1 ± 1.0 nm, respectively. Flake sizes and thicknesses were obtained from 100 flakes using AFM. e) Raman spectra from the three graphene samples. f) Film transmittance versus initial resistance for the three graphene samples. g) GF as a function of initial resistance for strain gauges made from the three different graphene samples. Dashed lines are linear fitting to the data. h) AFM images of EE, EE-small, and SE graphene samples deposited on SiO2/Si wafers, as well as EE graphene wrinkles right after being deposited on PET substrate (lower right).

the out-of-plane resistance due to changes of the overlap area are dominating the strain response. Large flakes exhibit large overlapping areas to neighboring flakes and their out-of-plane resistance becomes less susceptible to strain-induced deformation. For small flakes, on the other hand, more interflake connections are required to form conduction pathways across the film. Therefore, out-of-plane conduction plays a more significant role in the overall conduction process. Moreover, comparing films from SE and EE-small flakes, we find that despite having close average flake sizes, there is still significant difference in GFs. We hypothesize that this is due to the existence of flakes as large as 300 nm in EE-small graphene samples (Figure 1b), which may dominate the conduction behavior of small flakes, and weaken the strain response. It is also possible that the difference in morphology and electronic structure of the two graphene samples could result in different out-of-plane resistances.

Furthermore, wrinkles are observed on AFM images of film composed of EE graphene (Figure 1h, lower right panel). It could be seen that these wrinkles still exist after strain and release (Figure S3, Supporting Information). We assume that the wrinkles tend to flatten and compensate the strain, so that interflake slide is bypassed and out-of-plane resistance change are suppressed. For smaller flakes, we have not observed any wrinkles under AFM imaging.

2.2. Enhancing the Out-of-Plane Resistance

The presented impact of material dimension and production methods emphasizes the importance of the out-of-plane resistance in enhancing the gauge factor of graphene-based strain sensors. We therefore attempt to enhance the gauge factor by increasing the out-of-plane resistance between graphene flakes. Our approach is based on inserting bipolar surfactant molecules in-between graphene flakes to increase their interlayer distance. In this case, we use sodium deoxycholate (SDOC) due to its demonstrated good adhesion to graphene basal plane.[29] The molecule has two hydroxyl groups and one charged carboxylate group creating one face that is hydrophilic and another face that is hydrophobic. Since graphene is hydrophobic, the hydrophobic face of the SDOC molecule will adhere to the graphene surface, as illustrated in **Figure 2**a. We expect that increasing the SDOC coverage from zero to one monolayer on graphene would lead to an increase of the overall out-of-plane resistance of the film since an increasing gap distance would result in a suppressed tunneling conduction between flakes. Using the SE graphene material, we add SDOC to the sample solution by 1/10, 1/5, and 1/2 fractions of the graphene weight, and the products are named SE+1/10SDOC, SE+1/5SDOC, and SE+1/2SDOC, respectively. As shown in Figure 2c, films made from SE+1/10DOC exhibit negligible difference in GF compared to those made from pure SE graphene. When increasing the SDOC ratio to 1/5 of graphene weight, there is a significant increase in GF. Especially for films with initial resistances between 10 kΩ and 1 MΩ, the GFs are enhanced twofold. However, further increase of the SDOC ratio to 1/2 of graphene by weight does not help to improve the GF compared to pure graphene.

Adding surfactant from 1/10 to 1/5 improves the gauge factor, but further addition to 1/2 decreases the gauge factor (Figure 2c). This GF improvement is attributed to several factors. First, increased surfactant concentration results in an increasing tunneling barrier width. Without surfactant, the increase of graphene film resistance under strain mainly originates from breakage of conduction pathways between two

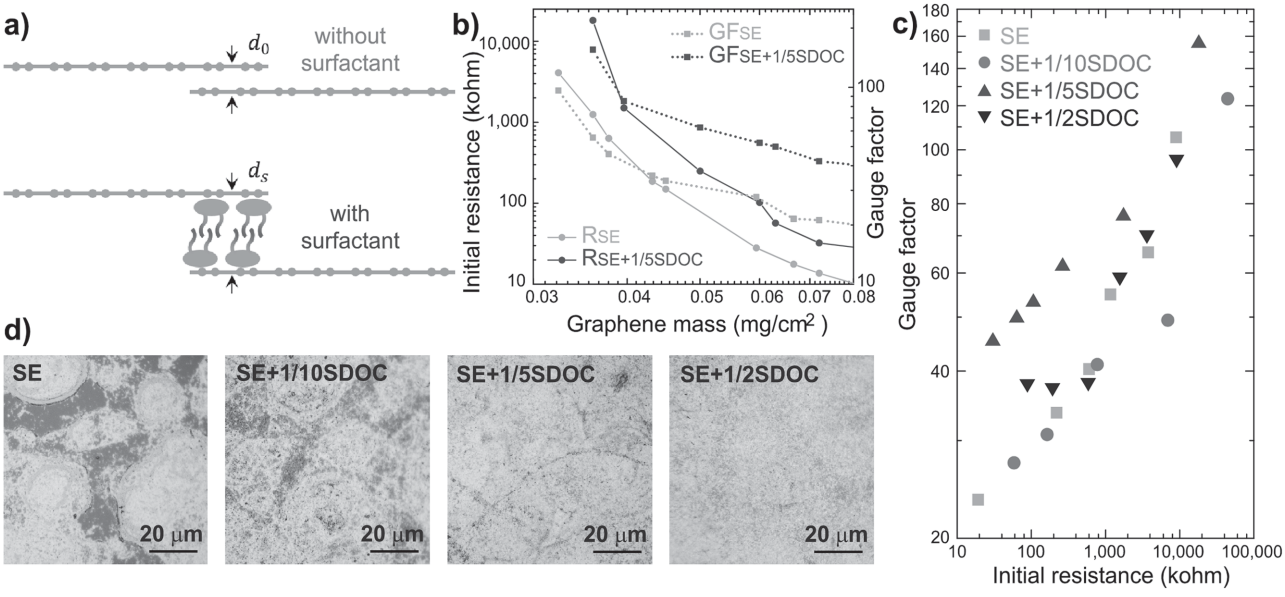

Figure 2. The effect of surfactant on GF. a) Schematic diagram of overlapping graphene flakes with and without surfactant molecules. b) Initial resistance and gauge factor as a function of graphene dosage for graphene with and without addition of surfactant. c) GF as a function of initial resistance for strain gauges made from the four different graphene samples. d) Optical Microscope images showing the morphology of the deposited graphene on the PET from the four different graphene solutions.

overlapping flakes. With the addition of the surfactant, especially when the concentration is large enough (>1/10), the tunneling resistance between the overlapping flakes increases and becomes more sensitive to the interlayer movements (this is the situation of the 1/5SDOC case where the GF is enhanced). However, as the SDOC concentration is further increased, the resistance of the SDOC molecules starts to dominate. This makes the percolative resistance less dominant and the gauge factor decreases, as observed in 1/2SDOC devices.

Moreover, we discovered that the film uniformity is also strongly affected by adding surfactant. Specifically, more surfactant leads to more uniform graphene film, as depicted in the optical microscopic image in Figure 2d. Without any surfactant, the film exhibits darker and lighter regions with obvious brightness contrast. Adding surfactant reduces the contrast between the darker and lighter regions. We assume the difference in graphene film uniformity originates from the variation in hydrophilicity of substrate surface affected by the surfactant molecules. The polyethylene terephthalate (PET) substrate is intrinsically moderate hydrophilic,[30] with a water contact angle around 70°. However, once surfactant molecules are sprayed onto PET, they effectively increase the hydrophilicity of the substrate by forming a self-assembled monolayer with exposed hydrophilic tail groups.

2.3. The Effect of Surface Treatment

To further verify the effect of substrate hydrophilicity on the film uniformity, we intentionally change the hydrophilicity of the PET surface, by treating it with O_2 plasma for 90 s (PLASMAPREEN II-862, 100 W). Before the O_2 plasma treatment, the water contact angle was measured to be 66.3° (**Figure 3**a). The optical microscopic (OM) image of the sprayed graphene film again shows obvious coffee ring patterns (Figure 3b). The edge of the ring appears lighter in color, while regions with lower graphene coverage look darker. The lighter color from the region with thick graphene stacks is due to the higher reflectance by the graphene stack compared to that of bare PET. The appearance of coffee rings reveals a series of droplet formation and evaporation.[31] However, after O_2 plasma treatment, the PET exhibit water contact angle of 13.1°, indicating near-perfect hydrophilicity. The graphene film on thus pretreated PET gives no coffee ring pattern, but shows homogeneous gray levels (Figure 3d), which are between the dark and light colors in Figure 3b. It is worth pointing out that the films in Figure 3b,d are from the same dosage of the same graphene ink.

To test if more uniform films can offer enhanced gauge factors, we fabricated strain gauges on PET with and without O_2 plasma treatment, respectively. The initial resistances of the strain gauges were varied from 40 MΩ to 10 kΩ, by increasing the amount of graphene dosage. It is obvious from **Figure 4**e that the gauges on more hydrophilic PET exhibit 20% to 90% higher GF, than those on pristine PET. The enhancement is universal across the whole range of tested initial resistances.

The uniformity is thought to affect the gauge factor as follows: When the deposition is not uniform, graphene flakes tend to aggregate in certain areas with several layers stacked on top of each other and it would be difficult to break the conduction pathways along these aggregates by straining the substrate. However, when the deposition is uniform across the substrate, the thickness of the film would be thinner and there exists more break points between flakes, thus giving higher gauge factors. It is worth noticing that even though O_2 plasma treatment offers near-perfect hydrophilicity, the resulting GF is still comparably lower than the GF of the sample made with an optimized amount of surfactant (Figure S4, Supporting Information), especially for lower initial resistance film with larger graphene dosage. We infer from this point that both higher hydrophilicity and larger out-of-plane resistance contribute to the improved GFs when surfactant is added.

2.4. Poly(methyl methacrylate) Encapsulation

Producing durable percolative graphene films is critical for practical application. Bare percolative graphene films exposed to the ambient are not very durable since graphene does not

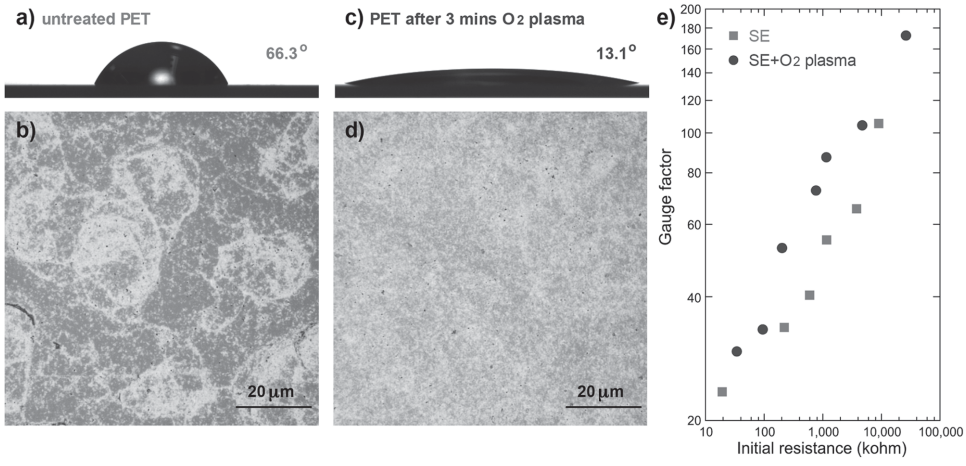

Figure 3. Effect of substrate hydrophilicity on deposition and GF. a) Contact angle of untreated PET. b) OM image of graphene film on untreated PET substrate. c) Contact angle of O_2 plasma treated PET. d) OM image of graphene film on treated PET substrate. e) GF as a function of initial resistance for strain gauges fabricated on two kinds of substrates.

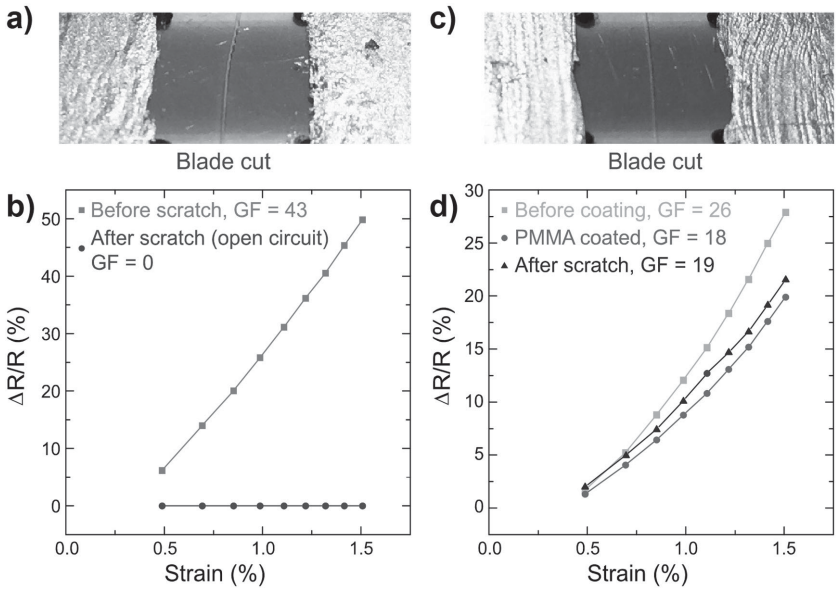

Figure 4. PMMA protection of graphene film. a) Strain gauge with graphene film exposed in the air. b) Resistance as a function of strain before and after scratch for unprotected graphene film. c) Strain gauge encapsulated with PMMA. d) Resistance as a function of strain before coating, after coating, and after scratch.

strongly adhere to the substrate or other graphene flakes. We verify this point by applying a 0.3 N cut across the graphene film using a razor blade. After the cut, a scratch mark can be observed (Figure 4a). By further testing the resistance of the film, we found that the conduction was interrupted, with a GF of 0 (Figure 4b). To increase the durability of the gauge, we encapsulate the percolative film with a thin layer of Poly(methyl methacrylate) (PMMA), produced by spin coating (Figure 4c). The PMMA is ≈5 µm thick, which maintains flexibility and can serve as a protection layer. After PMMA coating, the GF decrease from 26 to 18 (Figure 4d). We attribute this to the immobilization of the top few layers of graphene flakes by the PMMA. The immobilized graphene flakes cannot contribute to the strain-induced change of conduction pathways. To test the durability of the PMMA encapsulated gauge, we apply the same 0.3 N cut. Despite the obvious scratch mark (Figure 4c), the gauge factor remains unchanged (Figure 4d).

2.5. Integration of Flexible Transparent Pressure Sensor Array

We use the optimized graphene films to produce flexible transparent pressure sensor arrays based on a cavity design. Graphene strain gauges are deposited on thin PET films, which are suspended over a Polydimethylsiloxane (PDMS) chamber. Upon increase of external pressure P this cavity will decrease in volume and induce a deformation of the PET film. The resulting strain can be analyzed through the resistance change R of the graphene devices.

Our device consists of a PET substrate, percolative graphene film, metal contacts, and PDMS encapsulation, as shown in **Figure 5**a. First, Cr/Au metal contacts (10/100 nm) are deposited and patterned by a shadow mask on the PET substrate by thermal evaporation. Second, percolative graphene films are patterned using aerosol spray coating using a shadow mask. Each isolated film area can act as an active sensor. Third, a 5 µm thick PMMA protection layer is spin-coated. Finally, the graphene films are assembled on top of a PDMS chamber.

Figure 5b shows an optical photograph of a representative pressure sensor array, which presents excellent flexibility and transparency. Each of the red boxes indicates a region containing the percolative graphene film, or a sensing unit. When applying 0–60 kPa pressure to each of the four units, significant resistance change from the film was observed (Figure 5c). The sensitivity, as defined by $(\Delta R/R_0)/P$, was measured to be 0.20 ± 0.03 kPa^{-1} for the four units. This sensitivity is among the highest reported values for pressure sensors.[23,32,33] The sensitivity can easily be tuned by changing the dimensions of the PDMS chamber, the thickness of the PET substrate, and the

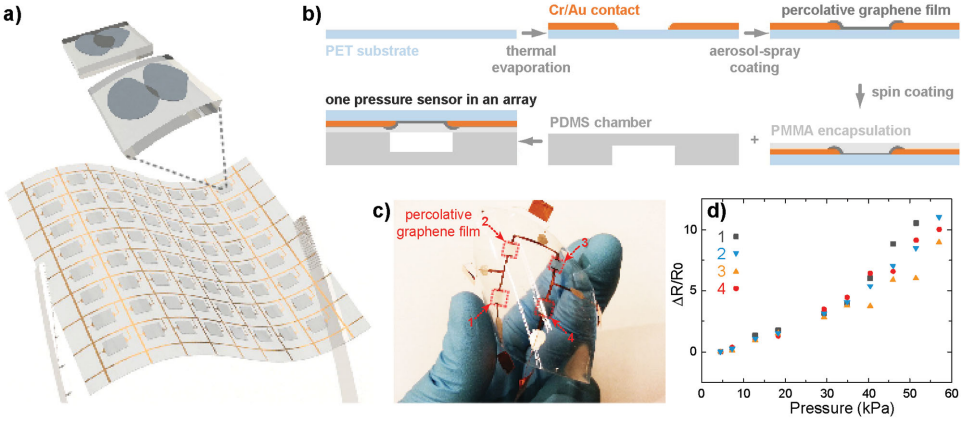

Figure 5. a) Schematics of the flexible, transparent pressure sensor array. b) Flow charts describing the fabrication of pressure sensor array. c) Pressure sensor array shows perfect transparency and flexibility. d) Resistance as a function of applied pressure of thus fabricated devices 1–4, as indicated in (c).

sensitivity of the graphene strain gauge. This tunable sensitivity allows application of the same device structure and fabrication method to various applications, from sensing a gentle touch to weighing an adult.

3. Conclusion

In conclusion, the guidelines to improved percolative graphene films for pressure sensing were explored. The study has revealed that the size of graphene flakes affects the GF, with smaller flakes yielding larger GF. This is attributed to the domination of out-of-plane conducting pathways in the percolative network. Furthermore, it was found that the GF could be enhanced twofold by introducing surfactant molecules into the graphene ink. The surfactant (a) increases the out-of-plane resistance and (b) improves the uniformity of the percolative graphene film. Based on these understanding, a two-by-two flexible and transparent pressure sensor array is demonstrated, with graphene flakes as the active sensing material. The array exhibits high flexibility, transparency, and reliable pressure response. Pressure between 0 and 60 kPa could be monitored using our devices with high reproducibility. This range represents pressures from as low as a gentle touch to as high as a normal person's weight on his/her footprint. The fabrication processes are facile, which include only shadow masking, thermal evaporation, aerosol spray coating, and spin coating. The flexible, transparent pressure sensor array and its fabrication processes are promising for advanced wearable electronics and bionics.

4. Experimental Section

Graphene flakes can be exfoliated from graphite using different techniques, including sonication[34,35] and shear force assisted solvent exfoliation,[25] electrochemical exfoliation,[36] and chemical conversion.[29,37] Different exfoliation techniques produce graphene flakes with different geometrical, chemical, and electrical properties.[30,28] To reveal the impact of exfoliation method and graphene property on their sensing performance, graphite is exfoliated using two different methods, namely sonication-assisted SE and EE.

To prepare SE graphene,[35] graphite (99.9%, Alfa Aesar #43319) was first dispersed at 10 mg mL^{-1} in 30 wt% Isopropyl alcohol (IPA) aqueous solution and then bath sonication (Branson 2510) was performed for 60 h. The obtained mixture was centrifuged twice at 12 000 g for 10 min. Each time the precipitate was discarded and the supernatant was kept. The resulting solution had a graphene concentration of 0.18 mg mL^{-1}.

EE graphene was prepared following the method developed by Khaled et al.[36] Briefly, graphite foil (99.8%, Alfa Aesar #43078) was used as anode in an electrochemical process under +10 V bias in 0.2 M K_2SO_4 + 0.1 M KOH aqueous solution. The resulting mixture was vacuum filtrated and redispersed to wash away the salts. The washing process was repeated four times with water and then twice with 30 wt% IPA. Finally, the mixture was centrifuged twice at 1000 g for 10 min to remove bulk graphite. The concentration of the resulting EE graphene in 30 wt% IPA aqueous solution was adjusted to 0.5mg mL^{-1}. Percolative graphene films (5 × 10 mm) were fabricated on flexible polyethylene terephthalate (PET, McMASTER-CARR, 8567K52, 0.178 mm thick) substrates by aerosol-spray deposition (Master Airbrush G23) of the graphene solution through a shadow mask. The percolative graphene films were subjected to uniaxial strain by uniformly bending the graphene coated PET substrates to a defined radius and the resistances along the strain axes were recorded (Figure S1, Supporting Information). The gauge factor for each film was calculated by $(\Delta R/R)/\varepsilon$, where $\Delta R/R$ was the normalized change in electrical resistance, and ε was the mechanical strain.

Supporting Information

Supporting Information is available from the Wiley Online Library or from the author.

Acknowledgements

The authors would like to acknowledge the support of HK ITC grant reference: ITS/195/14FP. After initial early view publication, Figures 1–4 were exchanged for optimized grayscale versions on July 25, 2016.

Received: August 30, 2015
Revised: January 11, 2016
Published online: May 9, 2016

[1] C. Pang, C. Lee, K. Y. Suh, *J. Appl. Polym. Sci.* **2013**, *130*, 1429.
[2] S. Takamatsu, T. Takahata, M. Muraki, E. Iwase, K. Matsumoto, I. Shimoyama, *J. Micromech. Microeng.* **2010**, *20*, 075017.
[3] H. K. Kim, S. Lee, K. S. Yun, *Sens. Actuators A-Phys.* **2011**, *165*, 2.
[4] F. R. Fan, L. Lin, G. Zhu, W. Z. Wu, R. Zhang, Z. L. Wang, *Nano Lett.* **2012**, *12*, 3109.
[5] J. Engel, J. Chen, C. Liu, *J. Micromech. Microeng.* **2003**, *13*, 359.
[6] J. Engel, J. Chen, Z. F. Fan, L. Chang, *Sens. Actuators A-Phys.* **2005**, *117*, 50.
[7] H. K. Lee, S. I. Chang, E. Yoon, *J. Microelectromech. Syst.* **2006**, *15*, 1681.
[8] K. Kim, K. R. Lee, D. S. Lee, N. K. Cho, W. H. Kim, K. B. Park, H. D. Park, Y. K. Kim, Y. K. Park, J. H. Kim, *J. Phys.: Conf. Ser.* **2006**, *34*, 399.
[9] K. Kim, K. R. Lee, W. H. Kim, K. B. Park, T. H. Kim, J. S. Kim, J. J. Pak, *Sens. Actuators A-Phys.* **2009**, *156*, 284.
[10] D. J. Lipomi, M. Vosgueritchian, B. C. K. Tee, S. L. Hellstrom, J. A. Lee, C. H. Fox, Z. N. Bao, *Nat. Nanotechnol.* **2011**, *6*, 788.
[11] G. Schwartz, B. C. K. Tee, J. G. Mei, A. L. Appleton, D. H. Kim, H. L. Wang, Z. N. Bao, *Nat. Commun.* **2013**, *4*, 1859.
[12] C. Wang, D. Hwang, Z. B. Yu, K. Takei, J. Park, T. Chen, B. W. Ma, A. Javey, *Nat. Mater.* **2013**, *12*, 899.
[13] M. Rothmaier, M. P. Luong, F. Clemens, *Sensors* **2008**, *8*, 4318.
[14] C. Pang, G. Y. Lee, T. I. Kim, S. M. Kim, H. N. Kim, S. H. Ahn, K. Y. Suh, *Nat. Mater.* **2012**, *11*, 795.
[15] L. Cai, L. Song, P. S. Luan, Q. Zhang, N. Zhang, Q. Q. Gao, D. Zhao, X. Zhang, M. Tu, F. Yang, W. B. Zhou, Q. X. Fan, J. Luo, W. Y. Zhou, P. M. Ajayan, S. S. Xie, *Sci. Rep.* **2013**, *3*, 3402.
[16] J. T. Muth, D. M. Vogt, R. L. Truby, Y. Menguc, D. B. Kolesky, R. J. Wood, J. A. Lewis, *Adv. Mater.* **2014**, *26*, 6307.
[17] S. Gong, W. Schwalb, Y. W. Wang, Y. Chen, Y. Tang, J. Si, B. Shirinzadeh, W. L. Cheng, *Nat. Commun.* **2014**, *5*, 3132.
[18] K. Ikeda, H. Kuwayama, T. Kobayashi, T. Watanabe, T. Nishikawa, T. Yoshida, K. Harada, *Sens. Actuators A-Phys.* **1990**, *21*, 146.
[19] A. Jornod, F. Rudolf, *Sens. Actuators* **1989**, *17*, 415.
[20] B. Morten, G. Decicco, M. Prudenziati, *Sens. Actuators A-Phys.* **1992**, *31*, 153.
[21] J. Zhou, Y. D. Gu, P. Fei, W. J. Mai, Y. F. Gao, R. S. Yang, G. Bao, Z. L. Wang, *Nano Lett.* **2008**, *8*, 3035.
[22] H. Tian, Y. Shu, Y. L. Cui, W. T. Mi, Y. Yang, D. Xie, T. L. Ren, *Nanoscale* **2014**, *6*, 699.

[23] A. D. Smith, F. Niklaus, A. Paussa, S. Vaziri, A. C. Fischer, M. Sterner, F. Forsberg, A. Delin, D. Esseni, P. Palestri, M. Ostling, M. C. Lemme, *Nano Lett.* **2013**, *13*, 3237.
[24] M. Hempel, D. Nezich, J. Kong, M. Hofmann, *Nano Lett.* **2012**, *12*, 5714.
[25] K. R. Paton, E. Varrla, C. Backes, R. J. Smith, U. Khan, A. O'Neill, C. Boland, M. Lotya, O. M. Istrate, P. King, T. Higgins, S. Barwich, P. May, P. Puczkarski, I. Ahmed, M. Moebius, H. Pettersson, E. Long, J. Coelho, S. E. O'Brien, E. K. McGuire, B. M. Sanchez, G. S. Duesberg, N. McEvoy, T. J. Pennycook, C. Downing, A. Crossley, V. Nicolosi, J. N. Coleman, *Nat. Mater.* **2014**, *13*, 624.
[26] I. I. Trusov, N. G. Askuntovich, R. P. Borovikova, M. A. Baklastov, V. P. Fedotov, *Phys. Lett. A* **1992**, *167*, 306.
[27] S. De, P. J. King, P. E. Lyons, U. Khan, J. N. Coleman, *ACS Nano* **2010**, *4*, 7064.
[28] Z. Y. Xia, S. Pezzini, E. Treossi, G. Giambastiani, F. Corticelli, V. Morandi, A. Zanelli, V. Bellani, V. Palermo, *Adv. Funct. Mater.* **2013**, *23*, 4684.
[29] S. C. Lin, C. J. Shih, M. S. Strano, D. Blankschtein, *J. Am. Chem. Soc.* **2011**, *133*, 12810.
[30] I. Donelli, P. Taddei, P. F. Smet, D. Poelman, V. A. Nierstrasz, G. Freddi, *Biotechnol. Bioeng.* **2009**, *103*, 845.
[31] R. D. Deegan, O. Bakajin, T. F. Dupont, G. Huber, S. R. Nagel, T. A. Witten, *Nature* **1997**, *389*, 827.
[32] S. E. Zhu, M. K. Ghatkesar, C. Zhang, G. C. A. M. Janssen, *Appl. Phys. Lett.* **2013**, *102*, 161904.
[33] H. B. Yao, J. Ge, C. F. Wang, X. Wang, W. Hu, Z. J. Zheng, Y. Ni, S. H. Yu, *Adv. Mat.* **2013**, *25*, 6692.
[34] Y. Hernandez, V. Nicolosi, M. Lotya, F. M. Blighe, Z. Y. Sun, S. De, I. T. McGovern, B. Holland, M. Byrne, Y. K. Gun'ko, J. J. Boland, P. Niraj, G. Duesberg, S. Krishnamurthy, R. Goodhue, J. Hutchison, V. Scardaci, A. C. Ferrari, J. N. Coleman, *Nat. Nanotechnol.* **2008**, *3*, 563.
[35] U. Halim, C. R. Zheng, Y. Chen, Z. Y. Lin, S. Jiang, R. Cheng, Y. Huang, X. F. Duan, *Nat. Commun.* **2013**, *4*, 2213.
[36] K. Parvez, Z. S. Wu, R. J. Li, X. J. Liu, R. Graf, X. L. Feng, K. Mullen, *J. Am. Chem. Soc.* **2014**, *136*, 6083.
[37] G. Eda, G. Fanchini, M. Chhowalla, *Nat. Nanotechnol.* **2008**, *3*, 270.